Analyzing second harmonic generation from arrays of cylinders using Dirichlet-to-Neumann maps

Lijun Yuan and Ya Yan Lu

Department of Mathematics, City University of Hong Kong, Kowloon, Hong Kong

We develop an efficient numerical method for analyzing second harmonic generation (SHG) in two-dimensional photonic crystals composed of nonlinear circular cylinders embedded in a linear background medium. Instead of solving the governing inhomogeneous Helmholtz equation for the second harmonic wave in the entire structure directly, we define and solve a locally generated second harmonic field in each cylinder (independent of all other cylinders), then merge the field together using Dirichlet-to-Neumann (DtN) maps of the unit cells. For linear waves in a unit cell without sources, the DtN map is an operator that maps the wave field to its normal derivative on the boundary and it can be approximated by a small matrix. A highly accurate pseudo-spectral method is used to solve the locally generated second harmonic wave in the cylinders. The method was applied to analyze enhanced SHG when the linear power reflectivity peaks at both the fundamental and second harmonic frequencies.

OCIS codes: 050.5298,190.2620,000.4430

1. Introduction

Due to the periodic variation of refractive index on the wavelength scale, photonic crystals (PhCs) [1] exhibit bandgaps and unusual dispersion behaviors. These properties give PhCs the unprecedented ability to control and manipulate light. Light can be confined at microcavities and waveguides created by defects in PhCs for frequencies in bandgaps. Unusual dispersion properties which give rise to superprism, ultrarefraction and slow light effects, also have many potential applications. Meanwhile, PhCs provide us an opportunity to enhance nonlinear optical effects for potential applications in all-optical signal processing. Second harmonic generation (SHG) [2] in one-dimensional multilayered media has been extensively studied [3]. Recent work [4–7] indicate that high conversion efficiency is possible for structures with doubly resonant cavities. For better lateral control and practical applications, it is important to analyze SHG in two or three dimensional structures. Furthermore,

two-dimensional (2D) PhCs offer additional degrees of freedom for phase-matching in SHG processes.

Numerical methods are essential to analyze SHG in photonic devices. In previous works [8–16], SHG in 2D PhCs have been studied using a number of different methods, including the Green's function method [8], the multipole method [12], integral equation method [14], the transfer matrix method [15] and nonlinear finite difference time domain (FDTD) method [16]. Meanwhile, a number of frequency domain numerical methods, such as the Fourier modal method [17], the bidirectional beam propagation method [19] and the eigenmode expansion method [20], have been used to analyze SHG in piecewise uniform waveguides. In a previous work [21], we developed a Dirichlet-to-Neumann (DtN) operator marching method for SHG in piecewise uniform waveguides. The method was originally developed for linear problems in 2D PhCs [22] and piecewise uniform waveguides [24]. For linear waves in a domain Ω without sources, the DtN map Λ is an operator that maps the wave field to its normal derivative on the boundary of Ω. For PhCs, the DtN maps of the unit cells can be approximated by small matrices and they allow us to avoid further computation in the interior of the unit cells [22]. For SHG problems, the governing equation for the second harmonic field is inhomogeneous. Therefore, the DtN map alone is not sufficient to characterize the field in the domain. However, it is still possible to localize the problem. Instead of solving the second harmonic field in the entire structure in one step, we can first calculate a locally generated second harmonic wave in each unit cell (independent of other cells) and then use the DtN maps to construct the solution for the entire structure. This approach was first used for SHG in piecewise uniform waveguides [21] where the "cells" are waveguide segments that are invariant along the waveguide axis. In the following sections, we extend this method to SHG in 2D PhCs composed of arrays of circular cylinders with $\chi^{(2)}$ nonlinearity.

2. Problem formulation

We consider 2D structures in the xy plane and assume that both the fundamental frequency and second harmonic waves are given in the transverse electric (TE) polarization. Therefore, the z-component of the electric field is the real part of $Ue^{-i\omega t} + Ve^{-2i\omega t}$, where ω is the angular frequency of the fundamental frequency wave. The governing equations for SHG are:

$$\partial_x^2 U + \partial_y^2 U + k_0^2 n^2(\mathbf{x};\omega)\, U = -k_0^2 \chi^{(2)}(\mathbf{x};\omega)\, \overline{U} V \tag{1}$$

$$\partial_x^2 V + \partial_y^2 V + 4k_0^2 n^2(\mathbf{x};2\omega)\, V = -2k_0^2 \chi^{(2)}(\mathbf{x};2\omega)\, U^2, \tag{2}$$

where $\mathbf{x} = (x, y)$, $\overline{U}$ is the complex conjugate of U, $k_0 = \omega/c$ is the free space wavenumber, c is the speed of light in vacuum, n is the linear refractive index function and $\chi^{(2)}$ is an element of the second-order nonlinear susceptibility tensor. We consider finite number of arrays of

cylinders in a linear background medium, where the cylinders are made of nonlinear $\chi^{(2)}$ material, and are infinitely long and parallel to the z axis. The structure is assumed to be periodic in the x direction with period a and bounded in the y direction by $0 < y < d$. For $y < 0$ and $y > d$, we have a linear non-dispersive medium with constant refractive index n_0.

For $y > d$, we specify a plane incident wave at frequency ω:

$$U^{(i)}(\mathbf{x}) = E_0 \exp\{i[\alpha_0^{(1)} x - \beta_0^{(1)}(y-d)]\}, \tag{3}$$

where E_0 is the amplitude of the incident wave, $\beta_0^{(1)} > 0$ and $[\alpha_0^{(1)}]^2 + [\beta_0^{(1)}]^2 = k_0^2 n_0^2$. Let the angle between the wave vector $(\alpha_0^{(1)}, -\beta_0^{(1)})$ and y axis be θ_0 (the angle of incidence), we have

$$\alpha_0^{(1)} = k_0 n_0 \sin(\theta_0), \quad \beta_0^{(1)} = k_0 n_0 \cos(\theta_0).$$

The transmitted and reflected waves for both frequencies can be written down as

$$\begin{aligned}
U^{(t)}(\mathbf{x}) &= E_0 \sum_{j=-\infty}^{+\infty} T_j^{(1)} \exp\{i[\alpha_j^{(1)} x - \beta_j^{(1)} y]\}, \quad y < 0, \\
U^{(r)}(\mathbf{x}) &= E_0 \sum_{j=-\infty}^{+\infty} R_j^{(1)} \exp\{i[\alpha_j^{(1)} x + \beta_j^{(1)} y]\}, \quad y > d, \\
V^{(t)}(\mathbf{x}) &= E_0 \sum_{j=-\infty}^{+\infty} T_j^{(2)} \exp\{i[\alpha_j^{(2)} x - \beta_j^{(2)} y]\}, \quad y < 0, \\
V^{(r)}(\mathbf{x}) &= E_0 \sum_{j=-\infty}^{+\infty} R_j^{(2)} \exp\{i[\alpha_j^{(2)} x + \beta_j^{(2)} y]\}, \quad y > d,
\end{aligned}$$

where $T_j^{(1)}$, $R_j^{(1)}$, $T_j^{(2)}$ and$R_j^{(2)}$ are unknown coefficients, and

$$\begin{aligned}
\alpha_j^{(1)} &= \alpha_0^{(1)} + 2j\pi/a, \qquad \beta_j^{(1)} = \sqrt{k_0^2 n_0^2 - [\alpha_j^{(1)}]^2}, \\
\alpha_j^{(2)} &= 2\alpha_0^{(1)} + 2j\pi/a, \qquad \beta_j^{(2)} = \sqrt{4k_0^2 n_0^2 - [\alpha_j^{(2)}]^2}.
\end{aligned}$$

The mathematical problem can be formulated in the rectangular domain Σ given by $0 < x < a$ and $0 < y < d$ [25]. With two properly defined operators $\mathcal{S}_1$ and $\mathcal{S}_2$ [22], we can write down the boundary conditions at $y = 0$ and $y = d$ as follows:

$$\partial_y U - i\mathcal{S}_1 U = -2i\beta_0^{(1)} E_0 \exp\{i\alpha_0^{(1)} x\}, \quad y = d, \tag{4}$$

$$\partial_y U + i\mathcal{S}_1 U = 0, \qquad y = 0, \tag{5}$$

$$\partial_y V - i\mathcal{S}_2 V = 0, \qquad y = d, \tag{6}$$

$$\partial_y V + i\mathcal{S}_2 V = 0, \qquad y = 0. \tag{7}$$

In the x direction, both wave fields are quasi-periodic:

$$U(x+a,y) = \mu U(\mathbf{x}), \qquad \partial_x U(x+a,y) = \mu\, \partial_x U(\mathbf{x}), \tag{8}$$

$$V(x+a,y) = \mu^2 V(\mathbf{x}), \qquad \partial_x V(x+a,y) = \mu^2 \partial_x V(\mathbf{x}), \tag{9}$$

where $\mu = \exp\{i\alpha_0^{(1)} a\}$ and $\mu^2 = \exp\{i2\alpha_0^{(1)} a\} = \exp\{i\alpha_0^{(2)} a\}$. Therefore, our problem is to determine the coefficients $T_j^{(1)}$, $R_j^{(1)}$, $T_j^{(2)}$ and $R_j^{(2)}$ by solving the nonlinear coupled Helmholtz equations (1) and (2) with boundary conditions (4-9).

If the conversion efficiency is not high, the undepleted-pump approximation is applicable. In that case, the effect of the second harmonic wave on the fundamental frequency field can be ignored. Eq. (1) is then replaced by the linear homogeneous Helmholtz equation:

$$\partial_x^2 U + \partial_y^2 U + k_0^2 n^2(\mathbf{x};\omega)\, U = 0 \tag{10}$$

and Eq. (2) for the second harmonic wave is a linear inhomogeneous equation. If the undepleted-pump approximation is not appropriate, the nonlinear equations (1) and (2) may be solved iteratively by replacing U and V in the right hand sides with their previous iterations, and using the solution of (10) as the first iteration. In the following, we assume that the undepleted-pump approximation is valid. However, our method for the inhomogeneous Helmholtz equation of V can also be used in the iterative scheme for solving the fully nonlinear SHG problem. For Eq. (10), an efficient method was developed in [22]. Therefore, we assume that the fundamental frequency wave is already solved and concentrate on the inhomogeneous Helmholtz equation (2) with boundary conditions (6), (7) and (9).

3. DtN operator marching

In principle, we can solve the second harmonic field V by standard numerical methods, such as the finite element method [26], with a direct discretization of the domain Σ. This gives rise to large, sparse, complex, non-Hermitian and indefinite linear systems that are expensive to solve. Special and more efficient methods can be developed by taking advantage of the available geometric features of the structure. For PhCs, the domain Σ can be divided into unit cells. Typically, there are only a small number of distinct unit cells and these cells have simple inclusions such as circular cylinders. The DtN operator marching method can take advantage of these special features. The method was first developed for linear waves in PhCs [22, 27, 28] and piecewise uniform waveguides [24]. In our earlier work [21], we extended the method to SHG in piecewise uniform waveguides. The method breaks the original problem of finding the second harmonic field in the entire structure into smaller and easier problems in each uniform waveguide segments by introducing locally generated second harmonic waves. For SHG in PhCs, although the basic steps remain the same, an efficient method for solving the inhomogeneous Helmholtz equation in circular geometry is needed.

As in [22], we divide the domain Σ is into m cells by lines of constant y. More precisely, we have $0 = y_0 < y_1 < ... < y_m = d$, so that the j-th cell Ω_j is given by $0 < x < a$ and $y_{j-1} < y < y_j$. For each y_j, we define two operators $\mathcal{Q}_j$ and $\mathcal{Y}_j$ and two functions $\varphi_j(x)$ and $\phi_j(x)$, such that

$$\mathcal{Q}_j V_j = \partial_y V_j - \varphi_j, \quad \mathcal{Y}_j V_j = V_0 + \phi_j, \tag{11}$$

where V is any solution of Eq. (2) satisfying boundary conditions (7) and (9), $V_j = V(x, y_j)$ and $\partial_y V_j = \partial_y V(x, y_j)$. In particular, φ_j and ϕ_j vanish if the right hand side of Eq. (2) is zero. Our method involves the following steps:

1. initialize $\mathcal{Q}_0$, $\mathcal{Y}_0$, ϕ_0 and φ_0 as

$$\mathcal{Q}_0 = -i\mathcal{S}_2, \quad \mathcal{Y}_0 = \mathcal{I}, \quad \varphi_0 = 0, \quad \phi_0 = 0, \tag{12}$$

   where $\mathcal{I}$ is the identity operator;

2. for $j = 0, 1, ..., m-1$,

   (a) calculate a local second harmonic field W in the nonlinear cylinder insider Ω_j,

   (b) find the DtN map Λ for Ω_j and the function f defined on the boundary of Ω_j,

   (c) find the reduced DtN map $\mathcal{M}$ and the boundary function g,

   (d) find $\mathcal{Q}_{j+1}$, $\mathcal{Y}_{j+1}$, ϕ_{j+1} and φ_{j+1} based on $\mathcal{M}$ and g;

3. solve V at $y = 0$ and $y = d$ from

$$(\mathcal{Q}_m - i\mathcal{S}_2)V_m = -\varphi_m, \quad V_0 = \mathcal{Y}_m V_m - \phi_m, \tag{13}$$

   where $V_m = V(x, d)$ and $V_0 = V(x, 0)$.

Compared with the original method for linear waves developed in [22], we need the functions ϕ_j, φ_j, f, g and the extra Step 2(a) to take care of the right hand side of Eq. (2). In our previous work for SHG in waveguides [21], Steps 2(a) and 2(b) are not needed, since we developed an efficient method for computing $\mathcal{M}$ and g directly. Notice that Step 1 comes from the boundary condition (7) and the definition (11). In Step 3, the boundary condition (6) and the definition (11) are used to find V_m and V_0, respectively.

Step 2 requires more explanations. For Step 2(a), if Ω_j contains a circular cylinder D with $\chi^{(2)}$ nonlinearity and the medium outside D is linear, we solve a locally generated second harmonic field W satisfying the same Helmholtz equation as V, i.e.,

$$\partial_x^2 W + \partial_y^2 W + 4k_0^2 n^2(\mathbf{x}; 2\omega)\, W = -2k_0^2 \chi^{(2)}(\mathbf{x}; 2\omega)\, U^2 \quad \text{in} \quad D \tag{14}$$

and a simple zero boundary condition $W = 0$ on ∂D (the boundary of D). An efficient numerical method for computing W is presented in Section 5.

In Step 2(b), we find the DtN map Λ and a function f, such that

$$\frac{\partial V}{\partial \nu} = \Lambda V + f \quad \text{on} \quad \partial\Omega_j, \tag{15}$$

for any V satisfying Eq. (2), where $\partial\Omega_j$ is the boundary of Ω_j and ν is a unit normal vector of $\partial\Omega_j$. Since Ω_j is a rectangle (or a square), we can explicitly write down V on the four edges of $\partial\Omega_j$. The normal derivative can be chosen as the x or y derivative on vertical or horizontal edges, respectively. If Λ and f are partitioned accordingly, Eq. (15) becomes

$$\begin{bmatrix} \partial_x V_{0j} \\ \partial_y V_{j+1} \\ \partial_x V_{1j} \\ \partial_y V_j \end{bmatrix} = \begin{bmatrix} \Lambda_{11} & \Lambda_{12} & \Lambda_{13} & \Lambda_{14} \\ \Lambda_{21} & \Lambda_{22} & \Lambda_{23} & \Lambda_{24} \\ \Lambda_{31} & \Lambda_{32} & \Lambda_{33} & \Lambda_{34} \\ \Lambda_{41} & \Lambda_{42} & \Lambda_{43} & \Lambda_{44} \end{bmatrix} \begin{bmatrix} V_{0j} \\ V_{j+1} \\ V_{1j} \\ V_j \end{bmatrix} + \begin{bmatrix} f_1 \\ f_2 \\ f_3 \\ f_4 \end{bmatrix}, \tag{16}$$

where $V_{j+1} = V(x, y_{j+1})$, $\partial_y V_{j+1} = \partial_y V(x, y_{j+1})$, $V_{0j} = V(0, y)$ and $V_{1j} = V(a, y)$. The details of this step are given in Section 4.

For Step 2(c), the operator $\mathcal{M}$ and the function g satisfy

$$\frac{\partial}{\partial y} \begin{bmatrix} V_{j+1} \\ V_j \end{bmatrix} = \mathcal{M} \begin{bmatrix} V_{j+1} \\ V_j \end{bmatrix} + \begin{bmatrix} g_1 \\ g_2 \end{bmatrix}, \tag{17}$$

where V satisfies Eq. (2) and quasi-periodic condition (9), g_1 and g_2 are the two components of g and they are functions of x. From the first and third equations of (16) and the quasi-periodic condition (9), we can eliminate $\partial_x V_{0j}$ and $\partial_x V_{1j}$ and solve for V_{0j} and V_{1j}. After that, we insert V_{0j} and V_{1j} into the second and fourth equations in (16) and obtain

$$\begin{aligned}
\mathcal{C}_1 &= \Lambda_{21} + \mu^2 \Lambda_{23}, \quad \mathcal{C}_2 = \Lambda_{41} + \mu^2 \Lambda_{43}, && (18)\\
\mathcal{D}_0 &= \Lambda_{31} + \mu^2 \Lambda_{33} - \mu^2 \Lambda_{11} - \mu^4 \Lambda_{13}, && (19)\\
\mathcal{D}_1 &= \mathcal{D}_0^{-1}(\mu^2 \Lambda_{12} - \Lambda_{32}), \quad \mathcal{D}_2 = \mathcal{D}_0^{-1}(\mu^2 \Lambda_{14} - \Lambda_{34}), && (20)\\
\mathcal{M} &= \begin{bmatrix} \mathcal{M}_{11} & \mathcal{M}_{12} \\ \mathcal{M}_{21} & \mathcal{M}_{22} \end{bmatrix} = \begin{bmatrix} \Lambda_{22} + \mathcal{C}_1 \mathcal{D}_1 & \Lambda_{24} + \mathcal{C}_1 \mathcal{D}_2 \\ \Lambda_{42} + \mathcal{C}_2 \mathcal{D}_1 & \Lambda_{44} + \mathcal{C}_2 \mathcal{D}_2 \end{bmatrix}, && (21)\\
g_1 &= \mathcal{C}_1 \mathcal{D}_0^{-1}(\mu^2 f_1 - f_3) + f_2, && (22)\\
g_2 &= \mathcal{C}_2 \mathcal{D}_0^{-1}(\mu^2 f_1 - f_3) + f_4. && (23)
\end{aligned}$$

For Step 2(d), using the definitions of $\mathcal{Q}_j$ and $\mathcal{Y}_j$, we can eliminate $\partial_y V_{j+1}$ and $\partial_y V_j$ in

(17) and obtain the following marching formulas:

$$\begin{aligned}
\mathcal{Z} &= (\mathcal{Q}_j - \mathcal{M}_{22})^{-1}\mathcal{M}_{21}, && (24)\\
h &= (\mathcal{Q}_j - \mathcal{M}_{22})^{-1}(g_2 - \varphi_j), && (25)\\
\mathcal{Q}_{j+1} &= \mathcal{M}_{11} + \mathcal{M}_{12}\mathcal{Z}, && (26)\\
\mathcal{Y}_{j+1} &= \mathcal{Y}_j\mathcal{Z}, && (27)\\
\varphi_{j+1} &= \mathcal{M}_{12}h + g_1, && (28)\\
\phi_{j+1} &= \phi_j - \mathcal{Y}_j h. && (29)
\end{aligned}$$

When x (for $0 < x < a$) is discretized by N points, $\mathcal{Q}_j$ and $\mathcal{Y}_j$ are approximated by $N \times N$ matrices, V_j, φ_j and ϕ_j are approximated by column vectors of length N. The number of operations required for each step is $O(N^3)$.

4. DtN map Λ and boundary function f

In this section, we consider a unit cell Ω, such as the Ω_j given by $0 < x < a$ and $y_{j-1} < y < y_j$ in Section 3, and describe our method for computing its DtN map Λ and the function f satisfying Eq. (15) on the boundary of Ω. We assume that a circular cylinder D made of homogeneous nonlinear material with a constant $\chi^{(2)}$ coefficient is located at the center of Ω, and the medium outside D is linear and homogeneous. At frequency 2ω, the refractive indices of D and D' are n_1 and n_2, respectively, where D' is the domain outside D but inside Ω. Denoting the boundaries of Ω and D by $\partial\Omega$ and ∂D, respectively, then the boundary of D' is the union of $\partial\Omega$ and ∂D.

The DtN map Λ is actually related to the homogeneous Helmholtz equation at frequency 2ω, i.e., Eq. (2) with a zero right hand side. Therefore, Λ can constructed following the approach used in [22]. We choose N_Ω points on $\partial\Omega$ (avoiding corners) and approximate the general solution of the homogeneous equation associated with Eq. (2) as a sum of N_Ω special solutions $\Phi_k(\mathbf{x})$ for $1 \le k \le N_\Omega$. Assuming that the points on $\partial\Omega$ are $\mathbf{x}_l$ for $1 \le l \le N_\Omega$, we calculate two $N_\Omega \times N_\Omega$ matrices Λ_1 and Λ_2 whose (l,k) entries are $\Phi_k(\mathbf{x}_l)$ and $\partial_\nu\Phi_k(\mathbf{x}_l)$, respectively, where $\nu = \nu(\mathbf{x}_l)$ is a unit normal vector of $\partial\Omega$ at $\mathbf{x}_l$. The DtN map Λ is then approximate by the matrix $\Lambda_2\Lambda_1^{-1}$. For unit cells containing circular inclusions, we can choose cylindrical waves as the special solutions.

To find the boundary function f, we need the DtN maps of D and D'. We first write down Eq. (2) in D and D' separately as

$$\begin{aligned}
\partial_x^2 V + \partial_y^2 V + 4k_0^2 n_1^2 V &= -2k_0^2\chi^{(2)}U^2, \quad \mathbf{x} \in D, && (30)\\
\partial_x^2 V + \partial_y^2 V + 4k_0^2 n_2^2 V &= 0, \qquad \mathbf{x} \in D'. && (31)
\end{aligned}$$

For domain D', we need its DtN map $\mathcal{A}$ satisfying

$$\begin{bmatrix} \partial_\nu V|_{\partial D} \\ \partial_\nu V|_{\partial\Omega} \end{bmatrix} = \mathcal{A} \begin{bmatrix} V|_{\partial D} \\ V|_{\partial\Omega} \end{bmatrix} = \begin{bmatrix} \mathcal{A}_{11} & \mathcal{A}_{12} \\ \mathcal{A}_{21} & \mathcal{A}_{22} \end{bmatrix} \begin{bmatrix} V|_{\partial D} \\ V|_{\partial\Omega} \end{bmatrix}, \tag{32}$$

where V is any solution of Eq. (31) and ν is a unit normal vector of the boundary. To find a matrix approximation of $\mathcal{A}$, we choose N_D points on ∂D, approximate the general solution of Eq. (31) by $N_\Omega + N_D$ special solutions and follow the approach described above. Since D is a circular disk, the special solutions in D' can be chosen as $J_j(2k_0 n_2 r)e^{ij\theta}$ and $Y_j(2k_0 n_2 r)e^{ij\theta}$, where (r, θ) are the polar coordinates with respect to the center of D, j is an integer, J_j and Y_j are Bessel functions of the first and second kinds. The DtN map $\mathcal{A}$ is approximated by an $(N_\Omega + N_D) \times (N_\Omega + N_D)$ matrix.

In the disk D, we decompose the second harmonic wave V as $V = S + W$, where W is a locally generated second harmonic wave and S satisfies the homogeneous Helmholtz equation

$$\partial_x^2 S + \partial_y^2 S + 4k_0^2 n_1^2 S = 0 \quad \text{in} \quad D. \tag{33}$$

Meanwhile, W satisfies the inhomogeneous Helmholtz equation

$$\partial_x^2 W + \partial_y^2 W + 4k_0^2 n_1^2 W = -2k_0^2 \chi^{(2)} U^2 \quad \text{in} \quad D \tag{34}$$

and a simple zero Dirichlet boundary condition $W|_{\partial D} = 0$. For domain D, we need the DtN map $\mathcal{B}$ such that

$$\partial_\nu S|_{\partial D} = \mathcal{B} S|_{\partial D} \tag{35}$$

for any S satisfying (34). An $N_D \times N_D$ matrix approximating $\mathcal{B}$ can be easily obtained based on representing the general solution of Eq. (33) as a linear combination of special solutions: $J_j(2k_0 n_1 r)e^{ij\theta}$. Since $V = S + W$ and $W|_{\partial D} = 0$, we have the following relationships:

$$\partial_\nu V|_{\partial D} = \partial_\nu S|_{\partial D} + \partial_\nu W|_{\partial D}, \quad S|_{\partial D} = V|_{\partial D}. \tag{36}$$

Using (35) and (36), we can eliminate terms $\partial_\nu V|_{\partial D}$ and $V|_{\partial D}$, and obtain

$$\Lambda = \mathcal{A}_{21}(\mathcal{B} - \mathcal{A}_{11})^{-1}\mathcal{A}_{12} + \mathcal{A}_{22}, \tag{37}$$

$$f = -\mathcal{A}_{21}(\mathcal{B} - \mathcal{A}_{11})^{-1}\partial_\nu W|_{\partial D}. \tag{38}$$

Eq. (37) is another way to calculate the DtN map Λ. Since Ω is composed of D and D', Λ can be obtained by merging the DtN maps of D and D'.

Therefore, if we have W (more precisely, $\partial_\nu W|_{\partial D}$), Λ and f can be easily calculated. The required number of operations is proportional to $(N_\Omega + N_D)^3$, but the integers N_Ω and N_D are typically quite small.

5. Locally generated second harmonic wave

In this section, we consider the locally generated second harmonic wave W satisfying the inhomogeneous Helmholtz Eq. (34) in D and the zero boundary condition $W|_{\partial D} = 0$, where D is a circular disk of radius δ. We present an efficient pseudo-spectral method [29] for computing W and $\partial_\nu W|_{\partial D}$. Our method involves the following steps:

1. re-write Eq. (34) in polar coordinates and extend the radial variable r to $(-\delta, \delta)$;
2. discretize r by a Chebyshev collocation method and obtain a system of ordinary differential equations (ODEs) in the angle variable θ;
3. use a linear transform to uncouple the system of ODEs;
4. solve the uncoupled ODEs;
5. reconstruct W and $\partial_r W|_{r=\delta}$ from the solutions of the uncoupled ODEs.

In a polar coordinate system where the center of D is the origin, Eq. (34) becomes

$$r^2 \frac{\partial^2 W}{\partial r^2} + r \frac{\partial W}{\partial r} + \frac{\partial^2 W}{\partial \theta^2} + 4 r^2 k_0^2 n_1^2 W = -2 r^2 k_0^2 \chi^{(2)} U^2 \tag{39}$$

for $0 \le r < \delta$ and $0 \le \theta \le 2\pi$. One way to overcome the singularity at $r = 0$ is to extend the radial variable r to $(-\delta, \delta)$ by

$$W(r, \theta) = W(-r, \tilde{\theta}), \quad \text{for } -\delta < r < 0 \text{ and } \tilde{\theta} = (\theta + \pi) \bmod (2\pi).$$

If the function U in the right hand side of (39) is similarly extended, then Eq. (39) is valid for $-\delta < r < \delta$ and $0 \le \theta \le 2\pi$.

We discretize the radial variable r by $r_k = -\delta \cos(k\pi/q)$ for $0 \le k \le q$. Notice that $r_0 = -\delta$ and $r_q = \delta$. To avoid $r = 0$, we assume q is an odd integer. For a smooth function of r, the derivative of that function at these $q+1$ points can be related to the function itself at these $q+1$ points by the Chebyshev differentiation matrix C. The second derivative with respect to r can be approximated by C^2. The explicit form of C can be found in [21, 29]. As a collocation method, Eq. (39) is assumed to be exactly valid at the $k-1$ interior points: r_k for $1 \le k < q$. Therefore, we need $\hat{C}$ and $\hat{D}$ which are the middle $(q-1) \times (q-1)$ blocks of C and C^2, respectively. In particular, we can write down C as

$$C = \begin{bmatrix} c_{00} & \tilde{c}_0 & c_{0q} \\ \vdots & \hat{C} & \vdots \\ c_{q0} & \tilde{c}_q & c_{qq} \end{bmatrix},$$

where $\tilde{c}_0$ and $\tilde{c}_q$ are row vectors of length $q-1$. Then, Eq. (39) is discretized as

$$\left(R^2\hat{D} + R\hat{C} + 4k_0^2 n_1^2 R^2\right)\vec{W} + \frac{d^2\vec{W}}{d\theta^2} = -2k_0^2\chi^{(2)}R^2\vec{F} \tag{40}$$

where

$$\vec{W} = \begin{bmatrix} W(r_1,\theta) \\ W(r_2,\theta) \\ \vdots \\ W(r_{q-1},\theta) \end{bmatrix}, \quad \vec{F} = \begin{bmatrix} U^2(r_1,\theta) \\ U^2(r_2,\theta) \\ \vdots \\ U^2(r_{q-1},\theta) \end{bmatrix}, \quad R = \begin{bmatrix} r_1 & & & \\ & r_2 & & \\ & & \ddots & \\ & & & r_{q-1} \end{bmatrix}$$

To uncouple the system (40), we diagonalize matrix $R\hat{C} + R^2\hat{D} + 4k_0^2 n_1^2 R^2$ as:

$$R^2\hat{D} + R\hat{C} + 4k_0^2 n_1^2 R^2 = P \begin{bmatrix} \lambda_1 & & & \\ & \lambda_2 & & \\ & & \ddots & \\ & & & \lambda_{q-1} \end{bmatrix} P^{-1}, \tag{41}$$

then, (40) becomes $q-1$ uncoupled second order ordinary differential equations

$$\frac{d^2\psi_k}{d\theta^2} + \lambda_k\psi_k = -2k_0^2\chi^{(2)}\tau_k(\theta), \quad 0 \le \theta < 2\pi \tag{42}$$

for $1 \le k < q$, where ψ_k and τ_k are the k-th components of $\vec{\psi}$ and $\vec{\tau}$ satisfying

$$P\vec{\psi} = \vec{W}, \quad P\vec{\tau} = \vec{F}.$$

If we discretize θ uniformly by p points, we can solve the equation by the Fourier spectral method using $O(p\log_2 p)$ operations [29]. To find $\partial_r W$ at $r = \delta$, we use the last row of the C matrix. Since $W = 0$ at $r = \pm\delta$, we have

$$\partial_r W|_{r=\delta} = \tilde{c}_q\vec{W} = b\vec{\psi}$$

where $b = [b_1, b_2, ..., b_{q-1}] = \tilde{c}_q P$. Since the extended function W is an even function, we have $\psi_k(\theta) = \psi_{q-k}(\tilde{\theta})$ for $1 \le k \le (q-1)/2$. Therefore,

$$\partial_r W(\delta,\theta) = \sum_{k=1}^{(q-1)/2} b_k\psi_{q-k}(\tilde{\theta}) + \sum_{k=(q-1)/2+1}^{q-1} b_k\psi_k(\theta).$$

Notice that we only need to solve Eq. (42) for $(q-1)/2$ different values of k.

6. Numerical examples

To illustrate our method, we analyze SHG by m arrays of nonlinear dielectric cylinders. The cylinders form a square lattice with a lattice constant a and they are surrounded by vacuum. The structure is finite in the y direction (given by $0 < y < d = ma$) and infinite and periodic in the x direction with period a. The parameters of the nonlinear cylinders are chosen as in [14]. We have the nonlinear coefficient $\chi^{(2)} = 2\,\mathrm{pm/V}$, the refractive index $n_1 = \sqrt{2}$ and the radius $\delta = 0.1a$. Since the background medium is vacuum, we have $n_0 = n_2 = 1$. A plane incident wave at frequency ω with the angle of incidence θ_0 is specified as in (3), where $E_0 = 10^6\,\mathrm{V/m}$. We study this problem for different values of the normalized frequency $\gamma = \omega a/(2\pi c) = k_0 a/(2\pi)$ and for different values of θ_0.

The case of one array, that is $m = 1$ and $d = a$, has been previously analyzed by a Green's function method with additional analytic approximations [14]. Although the structure is nearly transparent, strong reflection (for linear waves) is still possible at some frequencies depending on the angle of incidence. SHG can be significantly enhanced if strong reflections are observed at both ω and 2ω. Such a double resonance condition can only be satisfied at some specific angle of incidence. In Fig. 1, we show the linear power reflectivity for a plane

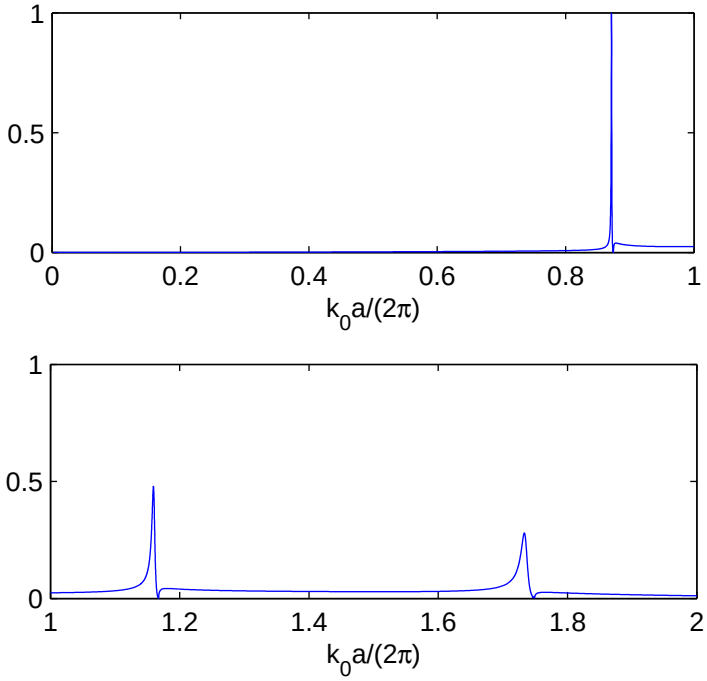

Fig. 1. Linear reflection spectrum for one array of cylinders, where the incident wave has a fixed angle of incidence $\theta_0 = 8.25^o$. The vertical axis is the power reflectivity defined in (43).

incident wave with an angle of incidence $\theta_0 = 8.25^o$. Mathematically, we are concerned with the homogeneous Helmholtz equation (10) subject to the boundary conditions (4,5,8). The power reflectivity is defined as

$$\text{P.R.} = \text{Re}\left[\sum_j \frac{\beta_j^{(1)}}{\beta_0^{(1)}} |R_j^{(1)}|^2\right], \tag{43}$$

where the sum contains only a few terms for which $\beta_j^{(1)}$ is real. For large $|j|$, $\beta_j^{(1)}$ is pure imaginary corresponding to evanescent waves. From Fig. 1, we observe a resonant reflection with nearly 100% reflectivity at $\gamma = 0.8714$ and a smaller reflection peak at twice that frequency. Therefore, we expect enhanced SHG when the fundamental frequency is given at $\gamma = 0.8714$. In Fig. 2, we show the normalized reflected power (power reflectivity) of the

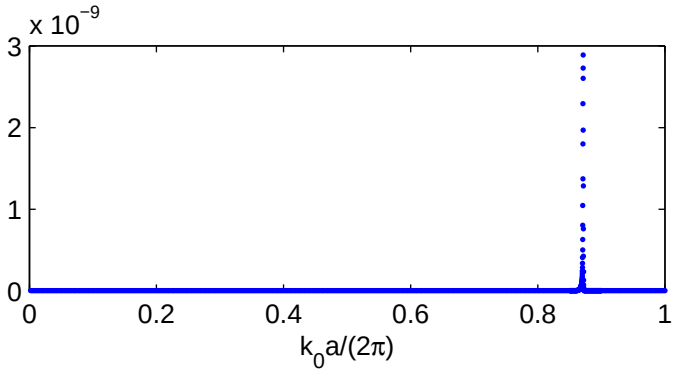

Fig. 2. Frequency dependence of the normalized reflected power of the second harmonic wave, defined in (44), for one array of cylinders. The angle of incidence the pump wave is fixed at $\theta_0 = 8.25^o$.

second harmonic wave as a function of γ. For the second harmonic wave, we define its power reflectivity as

$$\text{P.R.}^{(2)} = \text{Re}\left[\sum_j \frac{\beta_j^{(2)}}{\beta_0^{(1)}} |R_j^{(2)}|^2\right]. \tag{44}$$

Notice that the power of the reflected second harmonic wave is compared with the power of the incident field. A peak is clearly observed at $\gamma = 0.8714$ corresponding to the double resonance condition. In Fig. 3, we show the magnitudes of the fundamental frequency and second harmonic fields. Our results are consistent with the findings in [14]. The reflection peak and the enhanced SHG at $\gamma = 0.8714$ can be observed in Fig. 4 and Fig. 7 of [14], respectively. However, their results are presented for a fixed ratio between $\alpha_0^{(1)}$ (the x component of the incident wave vector) and $k_0 n_0$, thus the angle of incidence θ_0 varies with the frequency.

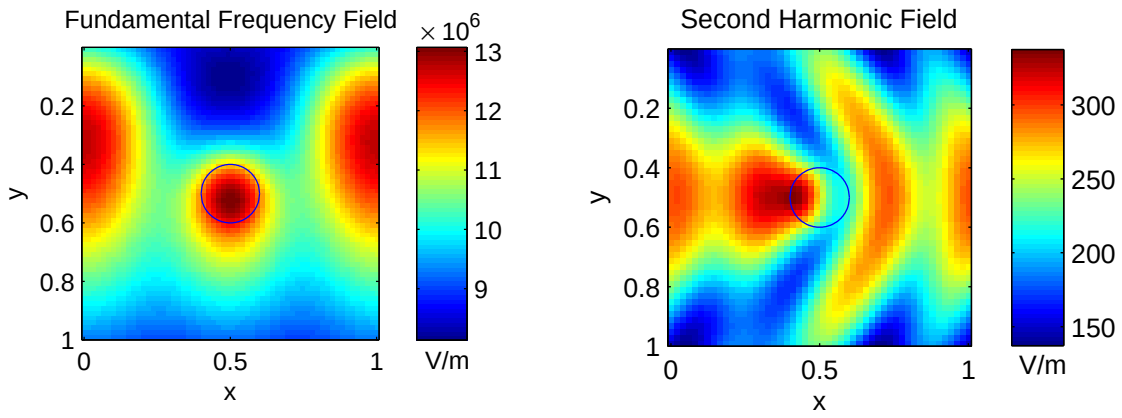

Fig. 3. Magnitudes of the fundamental frequency wave (left) and the second harmonic wave (right) for one array of cylinders at $\gamma = 0.8714$. The incident wave has a magnitude of 10^6 V/m and an angle of incidence $\theta_0 = 8.25^o$.

We have also implemented a nonlinear FDTD method as described in [18]. Because of the periodicity in the x direction, we also use a field-transformation technique presented in [30]. Using $\Delta x = \Delta y = 0.01a$ and $\Delta t = a/(250c)$, we are able to approximately reproduce the results in Fig. 1 and Fig. 2, including the locations of the peaks. However, the magnitudes of the peaks (at $\gamma = 0.8714$) are much lower in the FDTD results. We believe this is related to the limited resolution in our FDTD calculations and the possible shift of the double resonance condition due to errors in approximating the cylinder boundaries.

Expecting stronger SHG when more arrays are used, we consider the case of $m = 5$. First, we need to find a double resonance condition where reflectivity peaks at both ω and 2ω. This is possible when the angle of incidence is $\theta_0 = 7.6^o$. In Fig. 4, we show the linear power reflectivity as a function of γ for that θ_0. It is seen that a nearly 100% peak is reached at $\gamma = 0.86943$ and another peak is reached at double that frequency. The normalized reflected power of the second harmonic wave is shown in Fig. 5 as a function of γ. The result confirms that SHG is enhanced when the double resonance condition is satisfied. In Fig. 6, we show the magnitudes of both fundamental frequency and second harmonic fields. Notice that the second harmonic field has reached a few percent of the incident wave by magnitude. However, the power of the reflected second harmonic wave is only about one millionth of the power of the incident wave. This is so because the power is roughly proportional to the square of the magnitude and the second harmonic field is dominated by evanescent waves that are attached to the structure and do not contribute to the power reflectivity as defined in (44).

In the above calculations, we have used $N_\Omega = N_D = p = 36$ points to discretize the

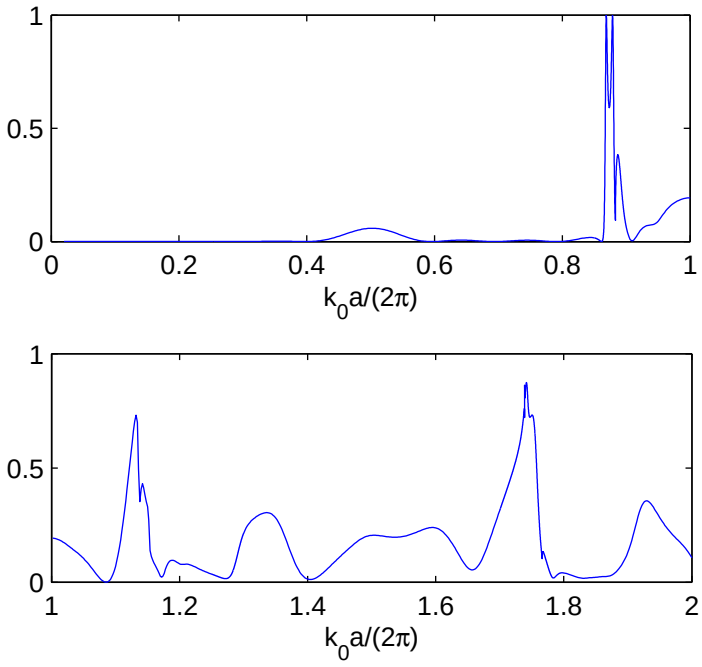

Fig. 4. Linear reflection spectrum for five arrays of cylinders, where the incident wave has a fixed angle of incidence $\theta_0 = 7.6^o$. The vertical axis is the power reflectivity defined in (43).

boundaries $\partial\Omega$, ∂D and the angle θ, and used $q = 31$ points to discretize the radial variable $r \in (-\delta, \delta)$. Since the unit cell is a square, the number of points on each edge is $N = 9$. Therefore, Q_j and Y_j are 9×9 matrices, ϕ_j and φ_j are column vectors of length 9. We are able to choose these small values for N_Ω and N_D, because the DtN maps are constructed from cylindrical waves and cylindrical wave expansions have exponential convergence rates. We are also able to use small p and q, since the locally generated second harmonic wave W is solved by a highly accurate pseudo-spectral method which also has an exponential convergence rate. The overall computation time scales linearly with the number of arrays m. For PhC structures with identical arrays, we only need to calculate the DtN maps $\mathcal{A}$, $\mathcal{B}$, Λ and $\mathcal{M}$ once. On the other hand, it is always necessary to solve the locally generated second harmonic field W in each unit cell, even when the unit cells are identical, since the right hand side of (2) is different on different unit cells. However, some preprocessing computing effort, such as the eigenvalue decomposition (41), does not need to be repeated.

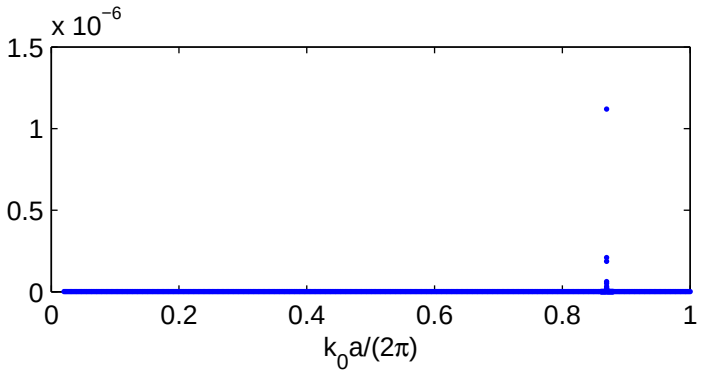

Fig. 5. Frequency dependence of the normalized reflected power of the second harmonic wave, defined in (44), for five arrays of cylinders. The angle of incidence the pump wave is fixed at $\theta_0 = 7.6^o$.

7. Conclusion

We have presented an efficient numerical method for analyzing SHG in arrays of nonlinear cylinders. The method was developed for SHG in 2D structures under the undepleted-pump approximation where the governing equation for the second harmonic wave is an inhomogeneous Helmholtz equation. Instead of solving the equation in the entire domain, we define and calculate a locally generated second harmonic field in each cylinder (independent of all other cylinders) and merge the solutions together using DtN maps of the unit cells. Our method is efficient, since the DtN maps can be approximated by small matrices and the locally generated second harmonic field can be solved by a highly accurate pseudo-spectral method. Although we have only used the method to analyze SHG in a PhC structure composed of m arrays of identical circular cylinders on a square lattice, our method is applicable to more general structures where different arrays may have different cylinders. The method can also be easily extended to structures on triangular lattices using the techniques developed in [28].

As in [14], we observe enhanced SHG when linear reflectivity peaks at both ω and 2ω. The overall second harmonic field is still quite weak for the structures we analyzed. The undepleted-pump approximation is certainly valid, since the second harmonic field was at most a few percent of the incident field by magnitude. However, our method should be useful for analyzing SHG in other PhC structures, including cases where the conversion efficiency is much higher. Our method for solving the inhomogeneous Helmholtz equation can be used iteratively to study fully nonlinear SHG problems without the undepleted-pump approximation.

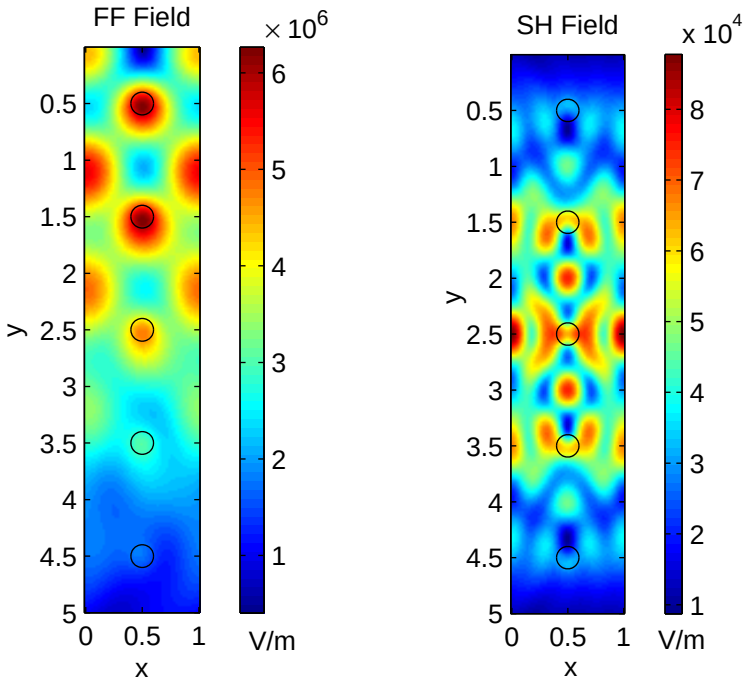

Fig. 6. Magnitudes of the fundamental frequency wave (left) and the second harmonic wave (right) for five arrays of cylinders at $\gamma = 0.86943$. The incident wave has a magnitude of 10^6 V/m and an angle of incidence $\theta_0 = 7.6^o$.

Acknowledgments

This research was partially supported by a grant from the Research Grants Council of Hong Kong Special Administrative Region, China (Project No. CityU 101706). Ya Yan Lu's e-mail address is mayylu@cityu.edu.hk.

References

1. J. D. Joannopoulos, R. D. Meade and J. N. Winn, *Photonic Crystals: Molding the Flow of Light*, Princeton University Press, Princeton, NJ. 1995.
2. M. M. Fejer, "Nonlinear optical frequency conversion," *Physics Today*, Vol. 47, pp. 25-32, 1994.
3. M. Bertolotti, "Wave interations in photonic band structures: an overview", *J. Opt. A: Pure Appl. Opt.*, Vol. 8, pp. S9-S32, 2006.
4. Z. Y. Ou and H. J. Kimble, "Enhanced conversion efficiency for harmonic-generation with double-resonance," Opt. Lett. **18**, 1053-1055 (1993).
5. F. F. Ren, R. Li, C. Cheng, H. T. Wang, J. R. Qiu, J. H. Si and K. Hirao, "Giant

enhancement of second harmonic generation in a finite photonic crystal with a single defect and dual-localized modes," Phys. Rev. B **70**, 245109 (2004).

6. M. Liscidini and L. C. Andreani, "Second-harmonic generation in doubly resonant microcavities with periodic dielectric mirrors," Phys. Rev. E **73**, 016613 (2006).
7. R. Li, J. Chen, Q. Xu, F. F. Ren, Y. X. Fan, J. Ding and H. T. Wang, "Saturation effect and forward-dominant second-harmonic generation in single-defect photonic crystals with dual localizations," Opt. Lett. **31**, 3327-3329 (2006).
8. K. Sakoda and K. Ohtaka, "Sum-frequency generation in a two-dimensional photonic lattice," Phys. Rev. B **54**, 5742-5749 (1996).
9. V. Berger, "Nonlinear photonic crystals," Phys. Rev. Lett. **81**, 4136-4139 (1998).
10. Y. Xu, R. K. Lee and A. Yariv, "Propagation and second-harmonic generation of electromagnetic waves in a coupled-resonator optical waveguide," J. Opt. Soc. Am. B **17**, 387-400 (2000).
11. E. Centeno, "Second-harmonic superprism effect in photonic crystals," Opt. Lett. **30**, 1054-1056 (2005).
12. E. Centeno and D. Felbacq, "Second-harmonic emission in two-dimensional photonic crystals," J. Opt. Soc. Am. B **23**, 2257-2264 (2006).
13. A. Arie, N. Habshoosh and A. Bahabad, "Quasi-phase matching in two-dimensional nonlinear photonic crystals," Opt. Quant. Electron. **39**, 361-375 (2007).
14. D. C. Marinica, A. G. Borisov and S. V. Shabanov, "Second harmonic generation from arrays of subwavelength cylinders," Phys. Rev. B **76**, 085311 (2007).
15. J. J. Li, Z. Y. Li and D. Z. Zhang, "Nonlinear frequency conversion in two-dimensional nonlinear photonic crystals solved by a plane-wave-based transfer-matrix method," Phys. Rev. B **77**, 195127 (2008).
16. R. Iliew, C. Etrich, T. Pertsch and F. Lederer, "Slow-light enhanced collinear second-harmonic generation in two-dimensional photonic crystals," Phys. Rev. B **77**, 115124 (2008).
17. W. Nakagawa, R. C. Tyan and Y. Fainman, "Analysis of enhanced second-harmonic generation in periodic nanostructures using modified rigorous coupled-wave analysis in the undepleted-pump approximation," J. Opt. Soc. Am. A **19**, 1919-1928 (2002).
18. Y. Dumeige, F. Raineri, A. Levenson and X. Letartre, "Second-harmonic generation in one-dimensional photonic edge waveguides," Phys. Rev. E **68**, 066617 (2003).
19. A. Locatelli, D. Modotto, C. De Angelis, F. M. Pigozzo and A. D. Capobianco, "Nonlinear bidirectional beam propagation method based on scattering operators for periodic microstructured waveguides," J. Opt. Soc. Am. B **20**, 1724-1731 (2003).
20. B. Maes, P. Bienstman and R. Baets, "Modeling second-harmonic generation by use of mode expansion," J. Opt. Soc. Am. B **22**, 1378-1383 (2005).

21. L. Yuan and Y. Y. Lu, "Dirichlet-to-Neumann map method for second harmonic generation in piecewise uniform waveguides," J. Opt. Soc. Am. B **24**, 2287-2293 (2007).
22. Y. Huang and Y. Y. Lu, "Scattering from Periodic Arrays of Cylinders by Dirichlet-to-Neumann Maps," J. Lightw. Technol. **24**, 3448-3453 (2006).
23. J. Yuan and Y. Y. Lu, "Photonic bandgap calculations using Dirichlet-to-Neumann maps," J. Opt. Soc. Am. A **23**, 3217-3222 (2006).
24. L. Yuan and Y. Y. Lu, "An efficient bidirectional propagation method based on Dirichlet-to-Neumann maps," IEEE Photon. Technol. Lett. **18**, 1967-1969 (2006).
25. G. Bao and Y. Chen, "A nonlinear grating problem in diffractive optics," SIAM J. Math. Anal. **28**, 322-337 (1997).
26. G. Bao Z. M. Chen and H. J. Wu, "Adaptive finite-element method for diffraction gratings", J. Opt. Soc. Am. A **22**, 1106-1114 (2005).
27. Y. Huang and Y. Y. Lu, "Modeling photonic crystals with complex unit cells by Dirichlet-to-Neumann maps," *Journal of Computational Mathematics* **25**, 337-349 (2007).
28. Y. Wu and Y. Y. Lu, "Dirichlet-to-Neumann map method for analyzing interpenetrating cylinder arrays in a triangular lattice," J. Opt. Soc. Am. B **25**, 1466-1473 (2008).
29. L. N. Trefethen, Spectral Methods in MATLAB, Society for Industrial and Applied Mathematics, 2000.
30. A. Taflove and S. C. Hagness, Computational Electrodynamics: the finite-difference time-domain method, Artech House, 2000.